Supporting Information

Rational design of ZrO_2-supported *d*-block single-atom electrochemical catalysts for the nitrogen reduction reaction

Kai Zhu,[a,b,c,d] Shaohua Lu*[a,b,c,d] and Xiaojun Hu*[a,b,c,d]

[a] College of Materials Science and Engineering, Zhejiang University of Technology, Hangzhou 310014, China.

[b] Institute of Wenzhou, Zhejiang University, Wenzhou 325006, China.

[c] Moganshan Diamond Research Center, Huzhou, 313200, China.

[d] Diamond Joint Research Center for Zhejiang University of Technology and Tanghe Scientific and Technology Company, Huzhou, 313200, China.

E-mail: lsh@zjut.edu.cn (Shaohua Lu); huxj@zjut.edu.cn (Xiaojun Hu)

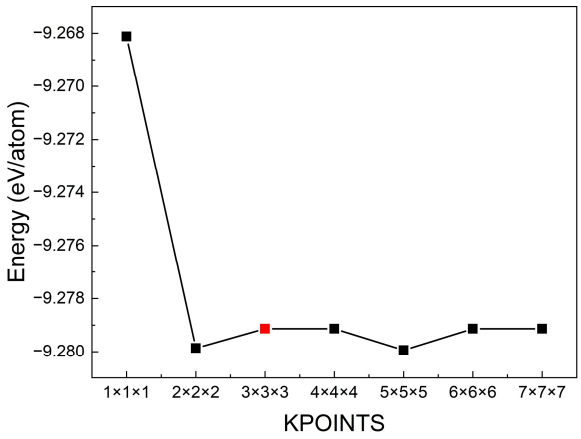

Figure S1. Energy convergence test for the K-points.

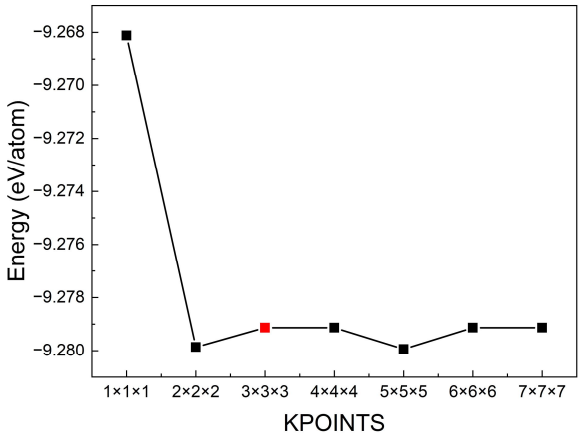

Figure S2. Energy convergence test for the K-points.

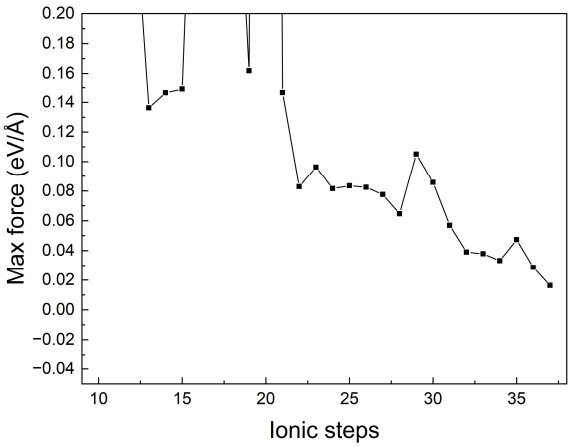

Figure S3. Maximum atomic force during structure optimization.

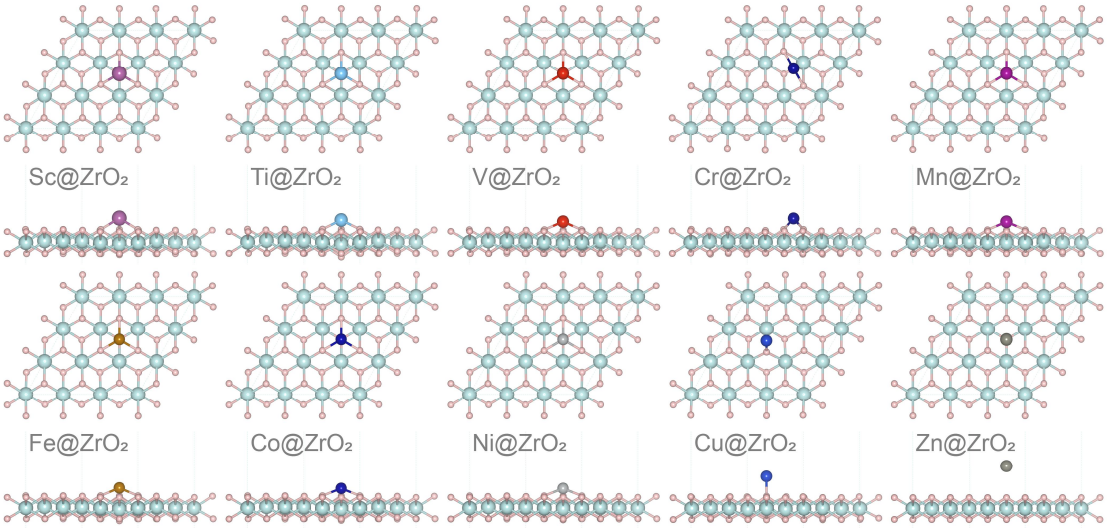

Figure S4. The top and side views of $TM@ZrO_2$ for 3d elements.

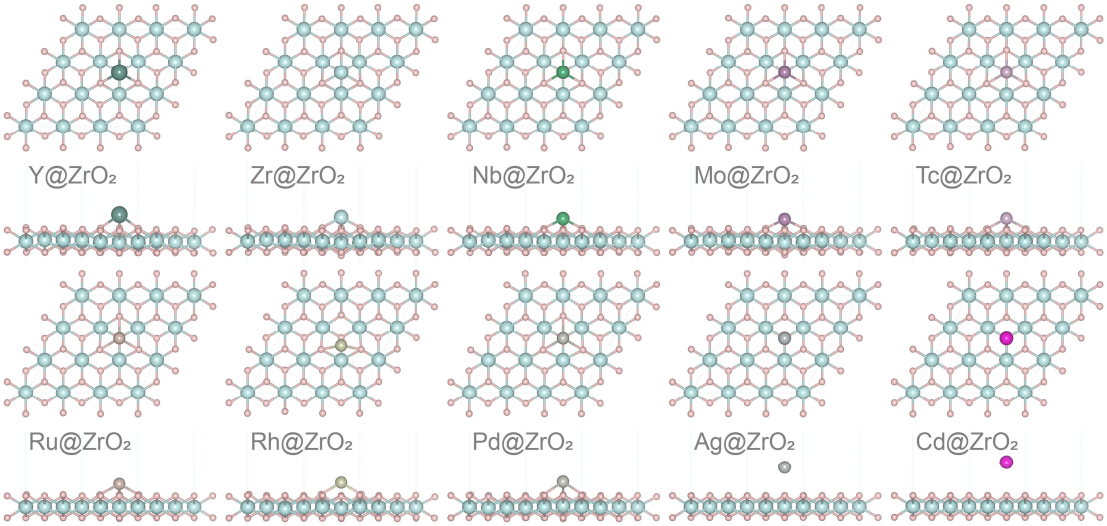

Figure S5. The top and side views of $TM@ZrO_2$ for 4d elements.

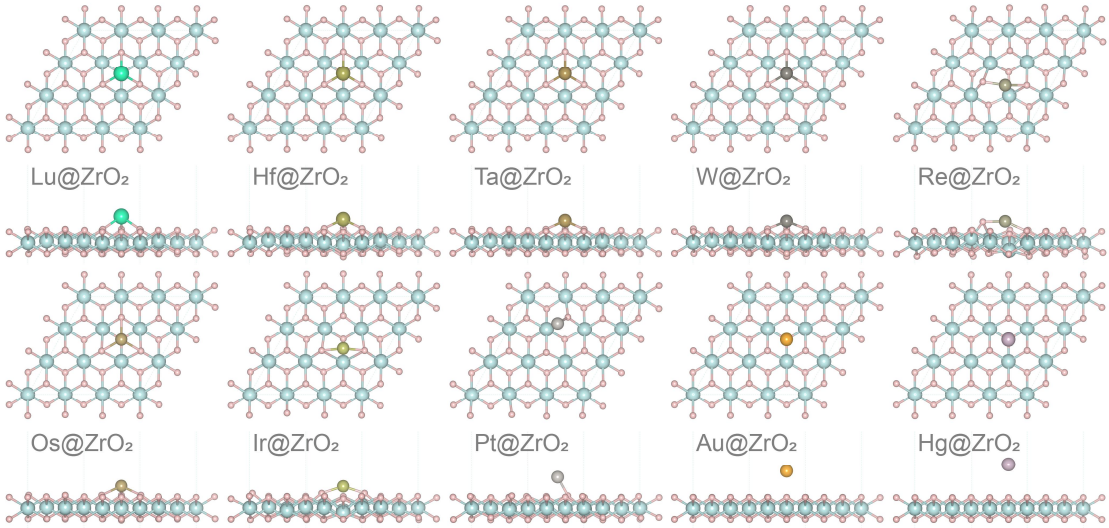

Figure S6. The top and side views of $TM@ZrO_2$ for 5d elements.

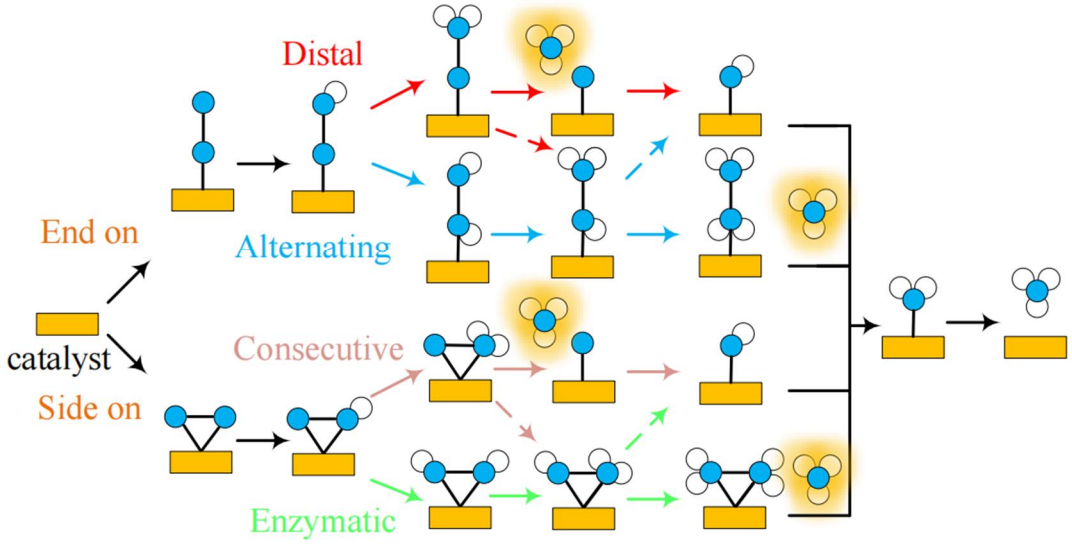

Figure S7. Possible reaction pathway for electrochemical reduction of N_2 to NH_3 molecule.

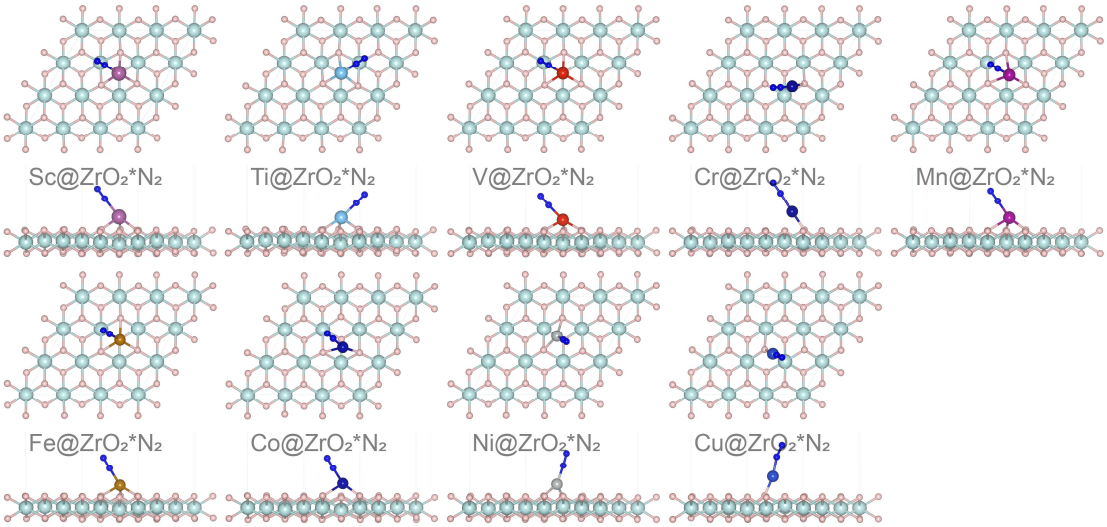

Figure S8. The top and side views of TM@ZrO_2*N_2 with end-on configuration for 3d elements.

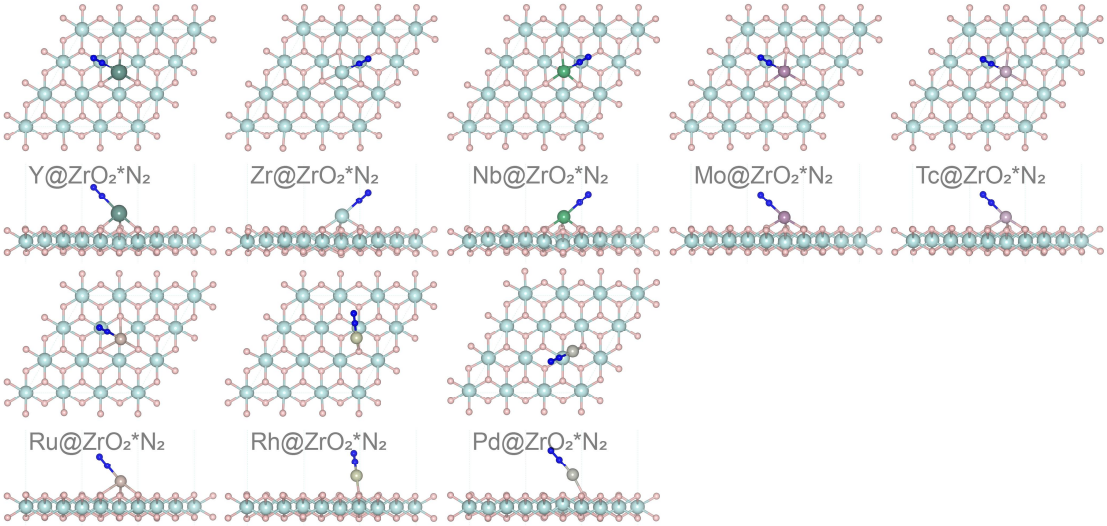

Figure S9. The top and side views of TM@ZrO_2*N_2 with end-on configuration for 4d elements.

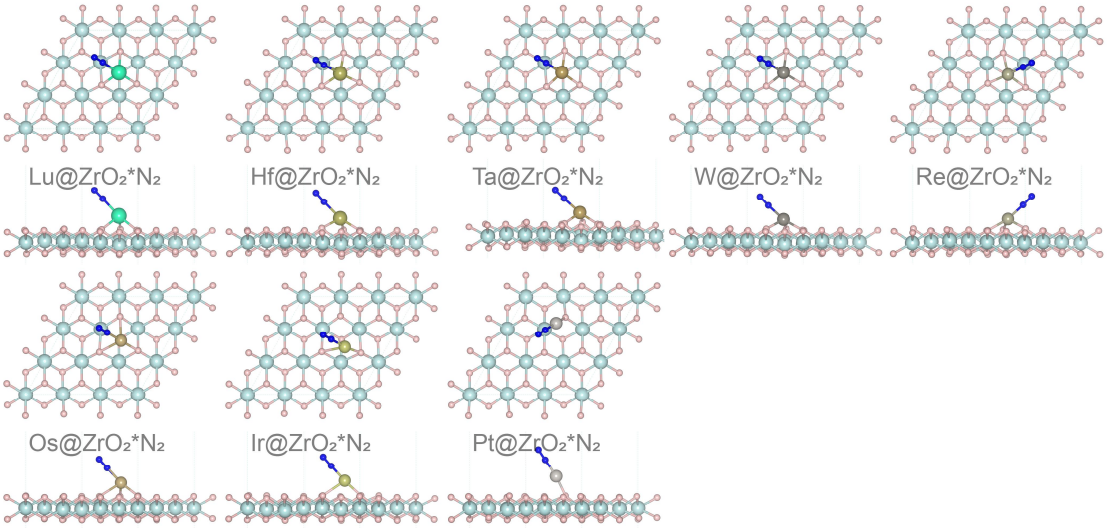

Figure S10. The top and side views of $TM@ZrO_2*N_2$ with end-on configuration for 5d elements.

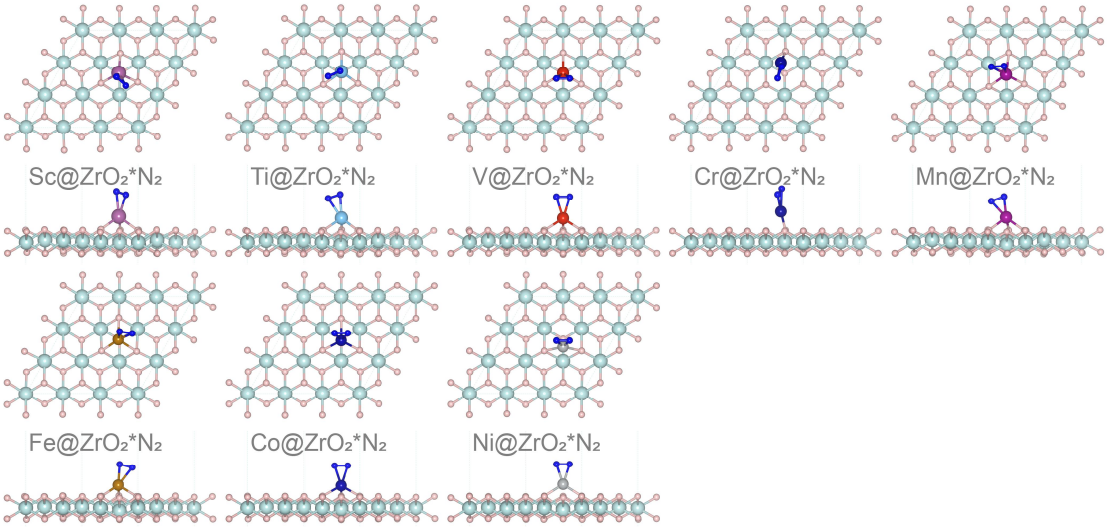

Figure S11. The top and side views of $TM@ZrO_2*N_2$ with side-on configuration for 3d elements.

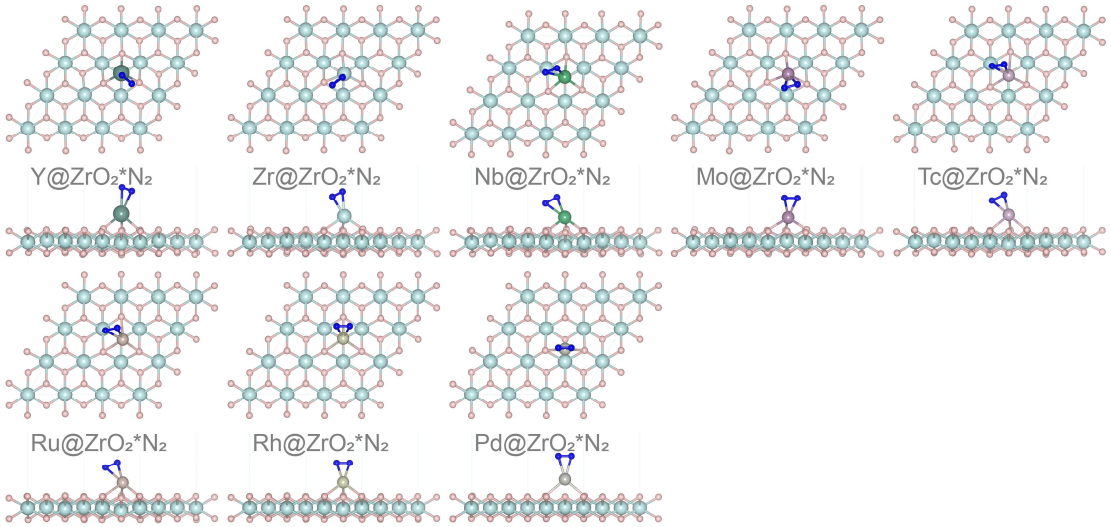

Figure S12. The top and side views of TM@ZrO_2*N_2 with side-on configuration for 4d elements.

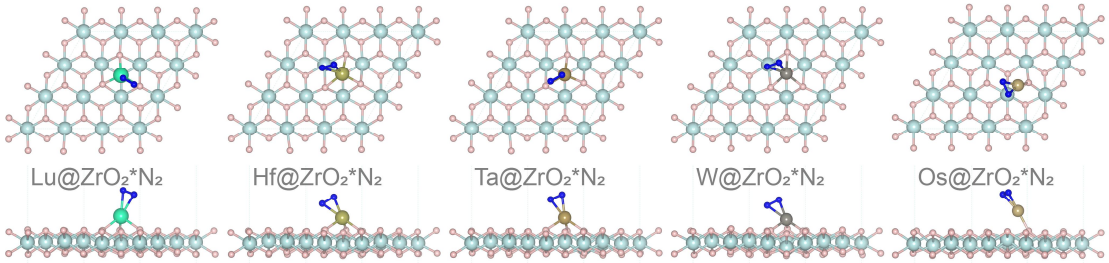

Figure S13. The top and side views of TM@ZrO_2*N_2 with side-on configuration for 5d elements.

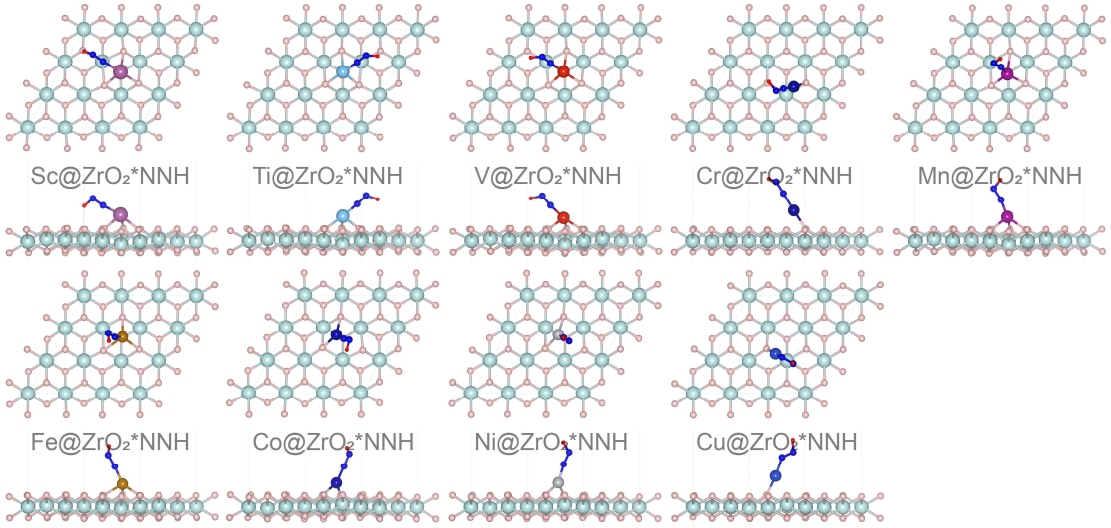

Figure S14. The top and side views of TM@ZrO_2*NNH for 3d elements.

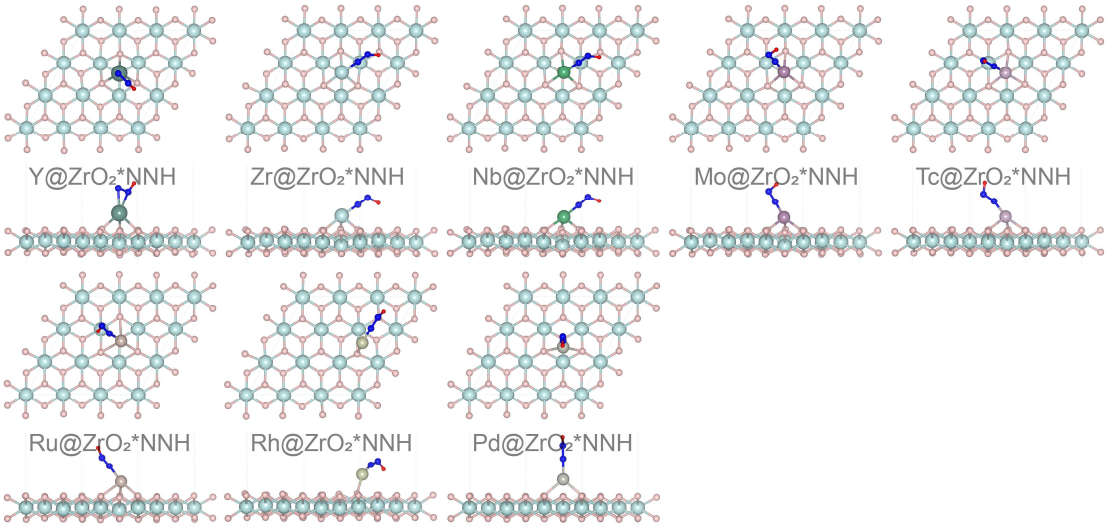

Figure S15. The top and side views of TM@ZrO_2*NNH for 4d elements.

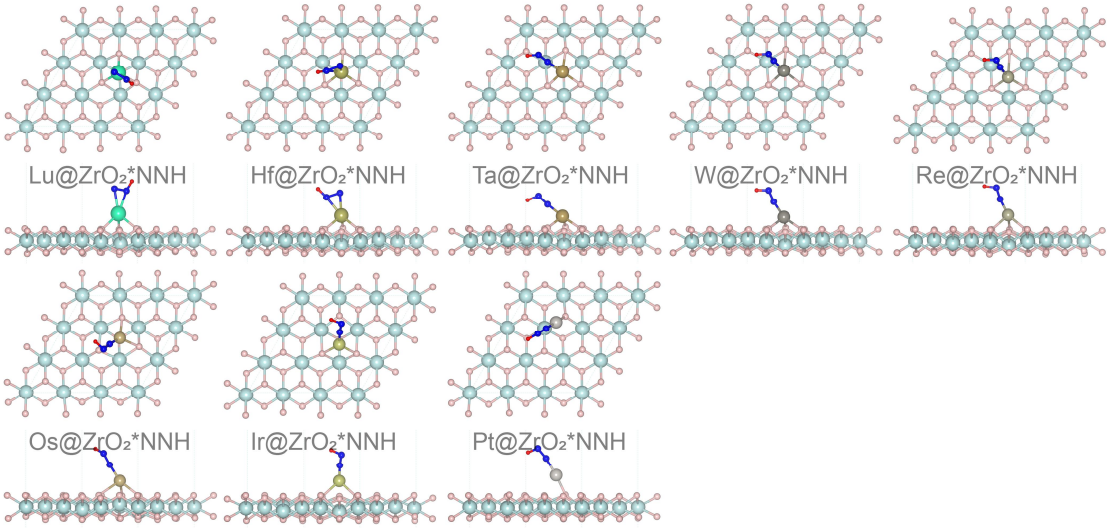

Figure S16. The top and side views of TM@ZrO_2*NNH for 5d elements.

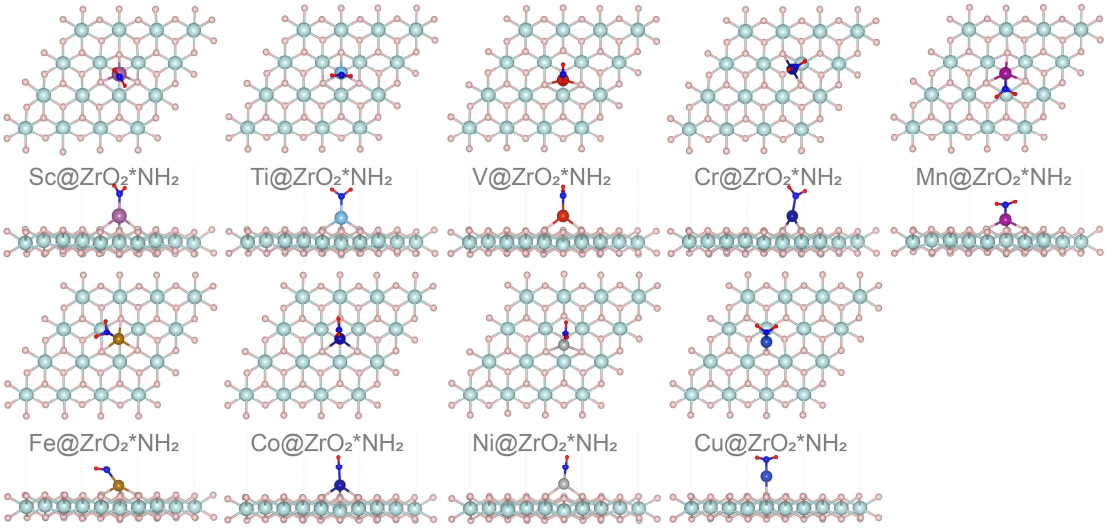

Figure S17. The top and side views of TM@ZrO_2*NH_2 for 3d elements.

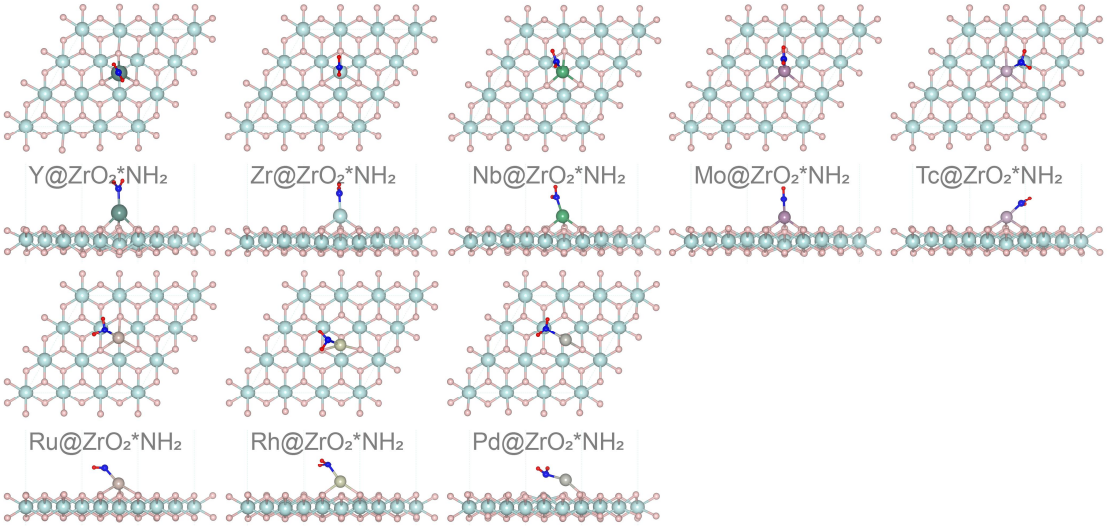

Figure S18. The top and side views of TM@ZrO_2*NH_2 for 4d elements.

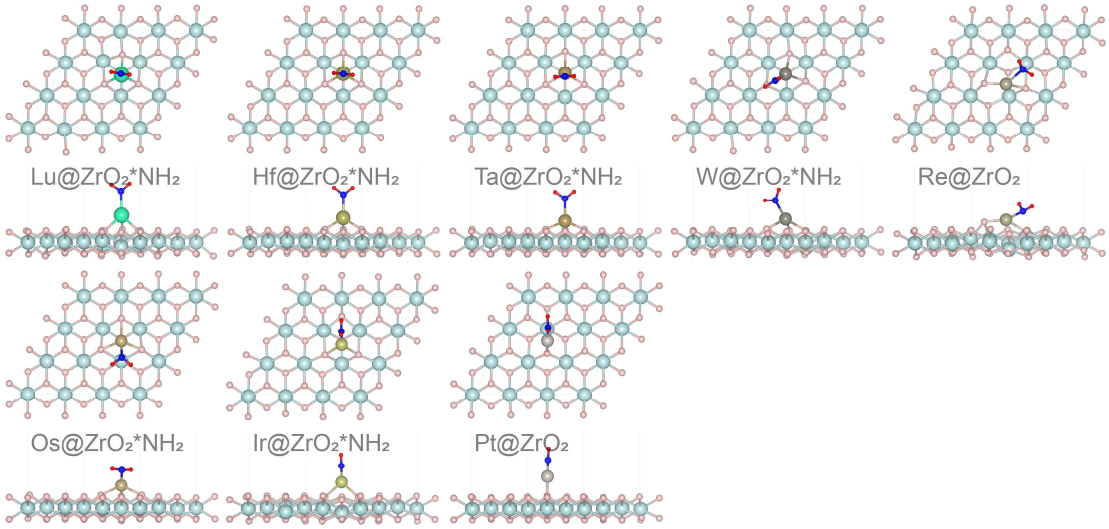

Figure S19. The top and side views of $TM@ZrO_2*NH_2$ for 5d elements.

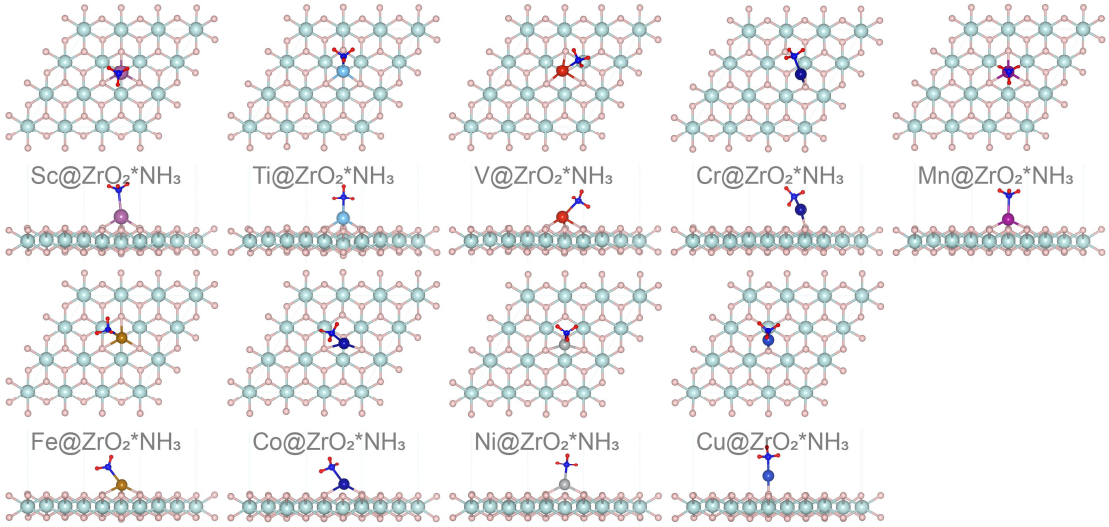

Figure S20. The top and side views of $TM@ZrO_2*NH_3$ for 3d elements.

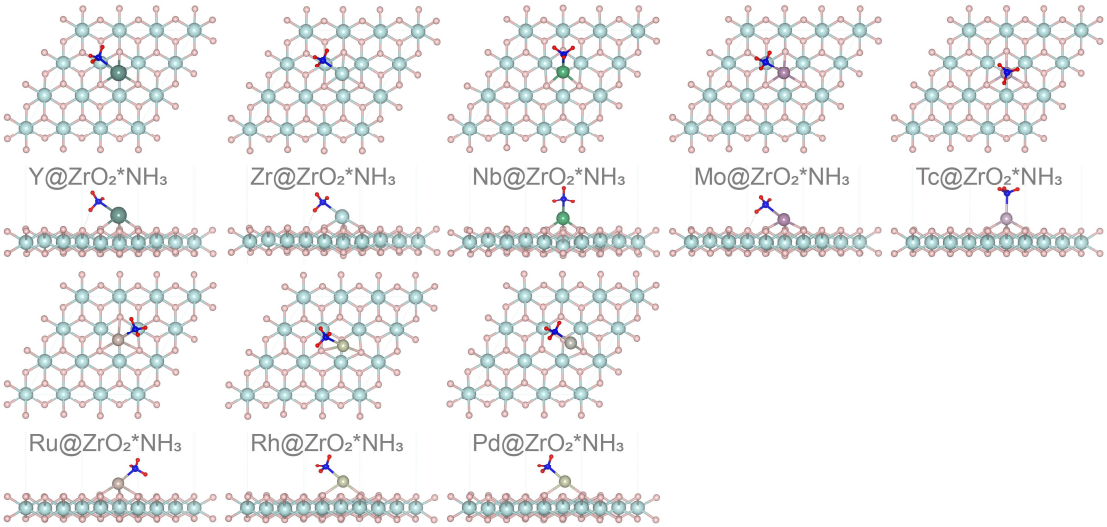

Figure S21. The top and side views of $TM@ZrO_2*NH_3$ for 4d elements.

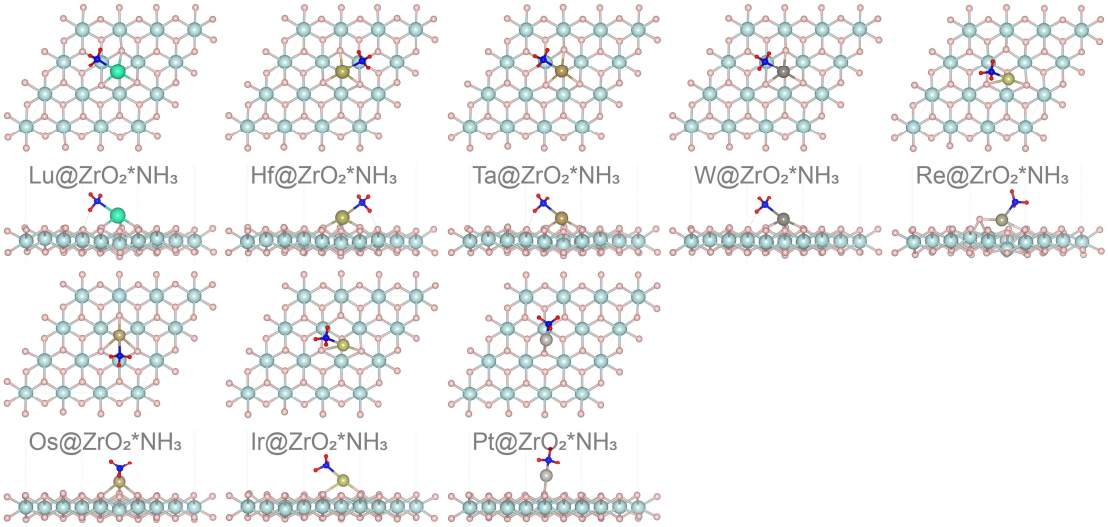

Figure S22. The top and side views of $TM@ZrO_2*NH_3$ for 5d elements.

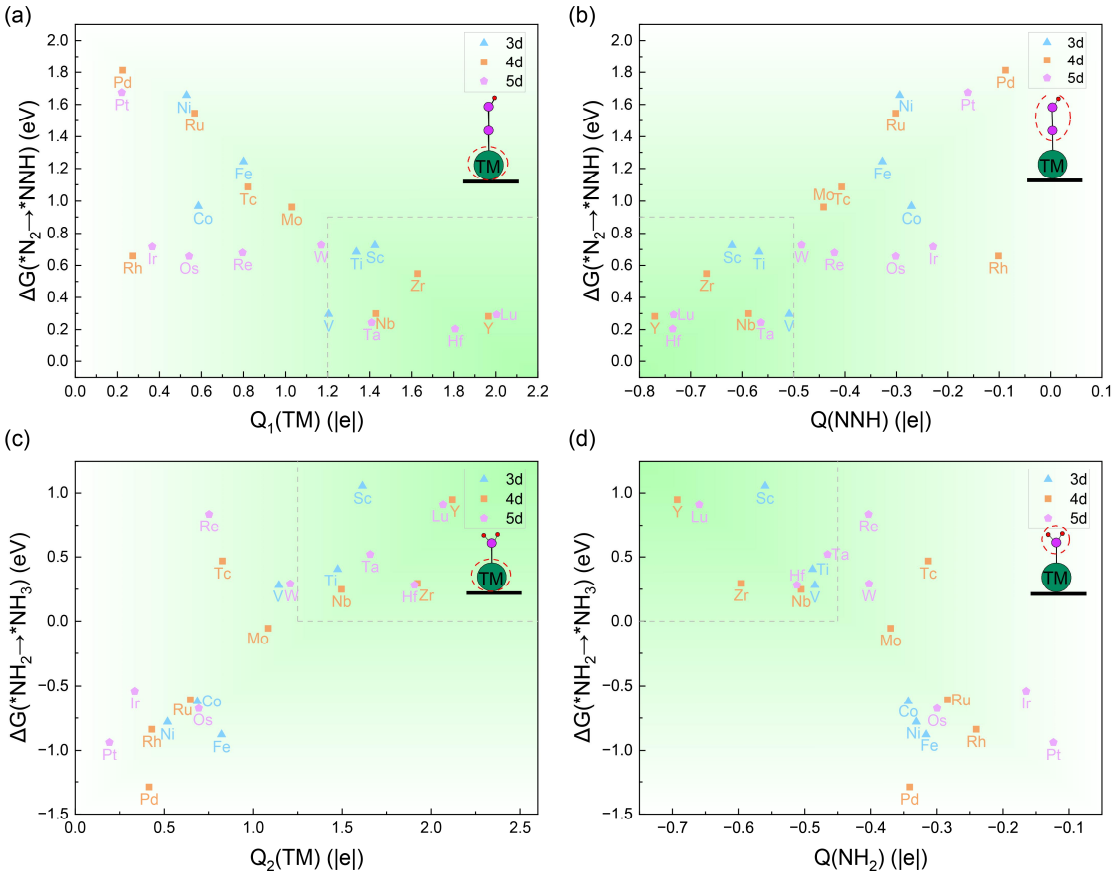

Figure S23. (a) Relationship between the Gibbs free energy difference from $*N_2$ to *NNH ($\Delta G(*N_2 \rightarrow *NNH)$) and the charge transfer of TM atom ($Q_1(TM)$), where $Q_1(TM)$ represents the charge transfer upon adsorption of the NNH moiety on the TM@ZrO_2 substrate. (b) Relationship between $\Delta G(*N_2 \rightarrow *NNH)$ and the charge transfer of the NNH moiety. (c) Relationship between the Gibbs free energy difference from $*NH_2$ to $*NH_3$ ($\Delta G(*NH_2 \rightarrow *NH_3)$) and the charge transfer of the TM atom ($Q_2(TM)$), where $Q_2(TM)$ represents the charge transfer upon adsorption of the NH_2 moiety on the TM@ZrO_2 substrate. (d) Relationship between $\Delta G(*NH_2 \rightarrow *NH_3)$ and the charge transfer of the NH_2 moiety.

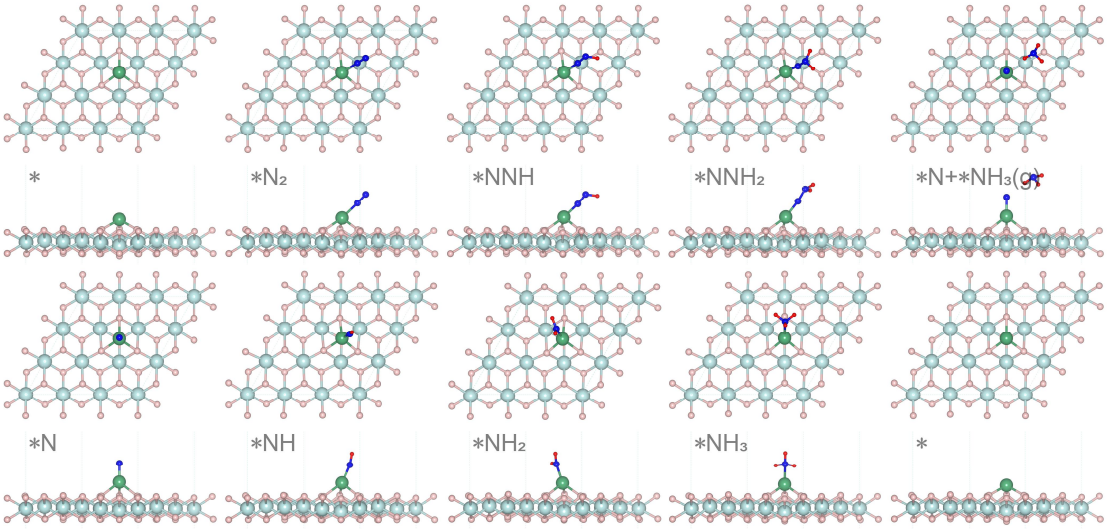

Figure S24. The NRR pathway of Nb@ZrO_2 with end-on configuration.

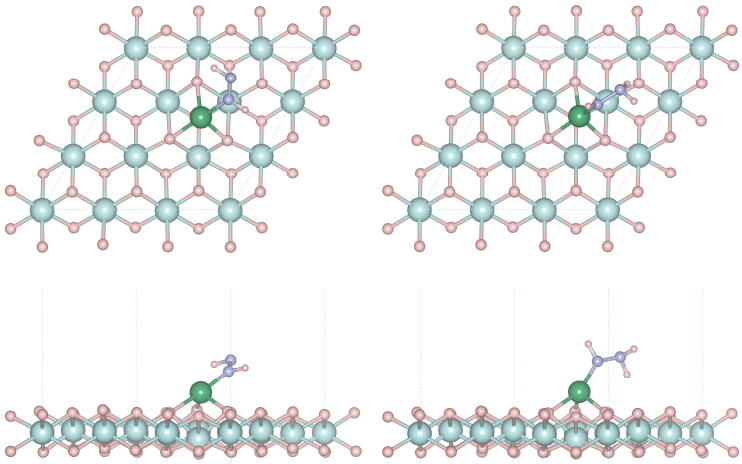

Figure S25. Top and side views of Nb@ZrO_2*NHNH and Nb@ZrO_2*$NHNH_2$.

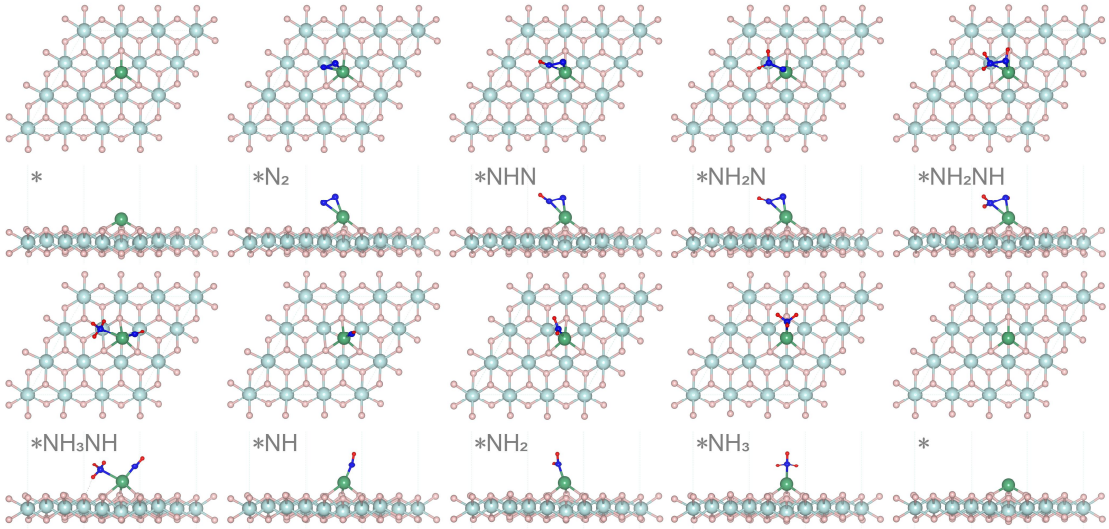

Figure S26. The NRR pathway of Nb@ZrO_2 with side-on configuration.

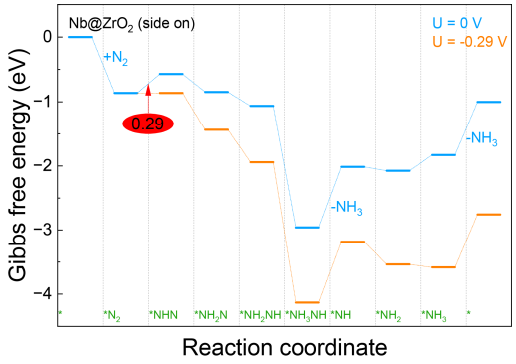

Figure S27. The free energy diagrams of Nb@ZrO_2 with side-on configuration.

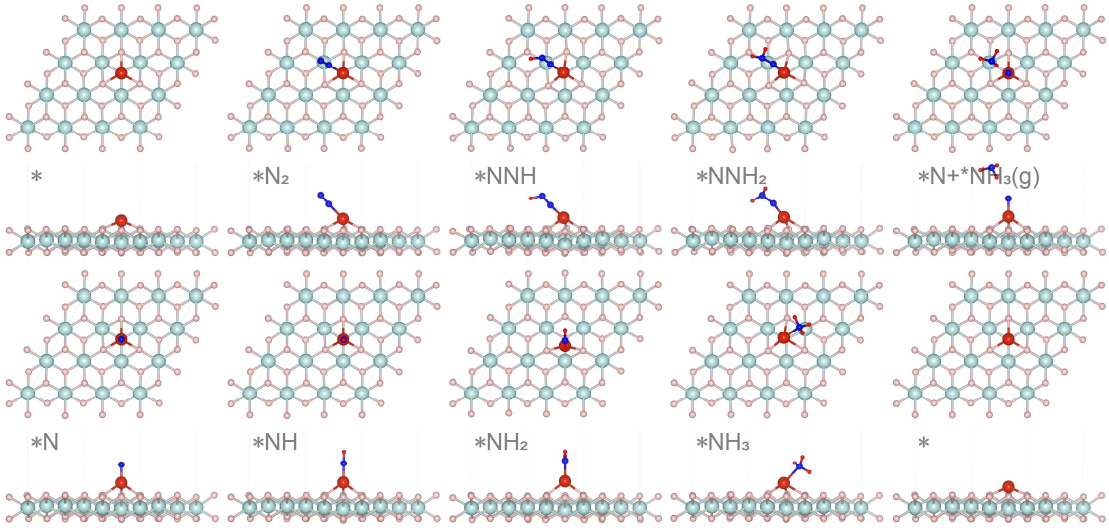

Figure S28. The NRR pathway of V@ZrO_2 with end-on configuration.

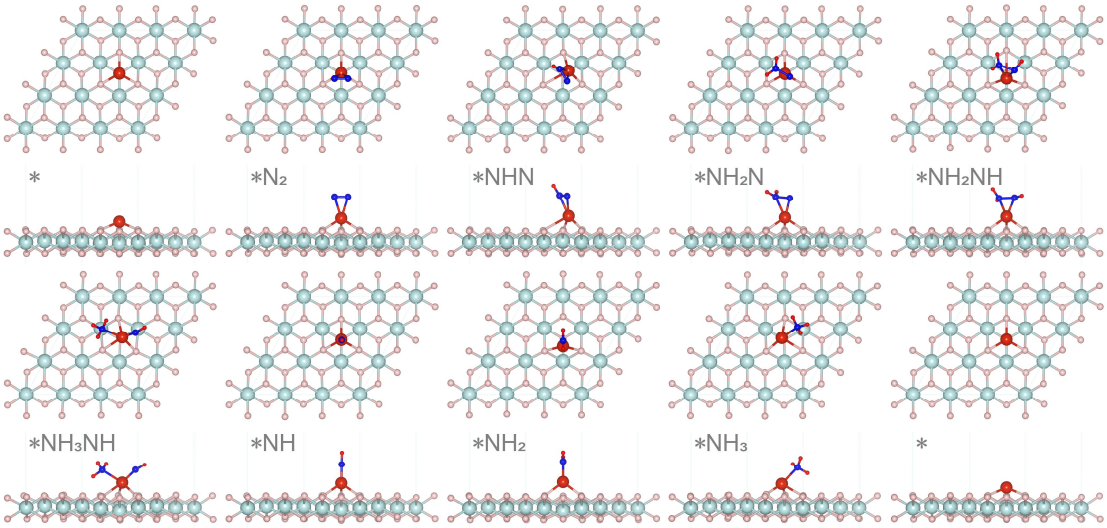

Figure S29. The NRR pathway of V@ZrO_2 with side-on configuration.

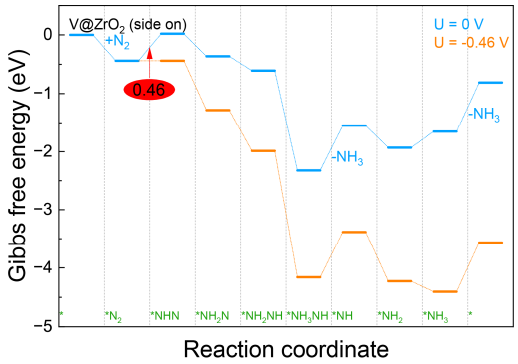

Figure S30. The free energy diagrams of V@ZrO_2 with side-on configuration.

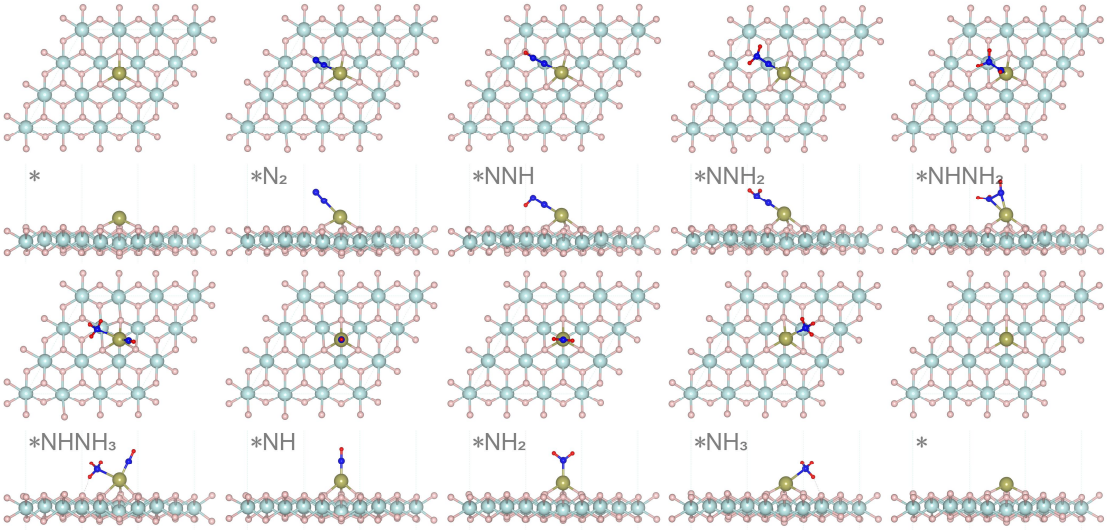

Figure S31. The NRR pathway of Hf@ZrO_2 with end-on configuration.

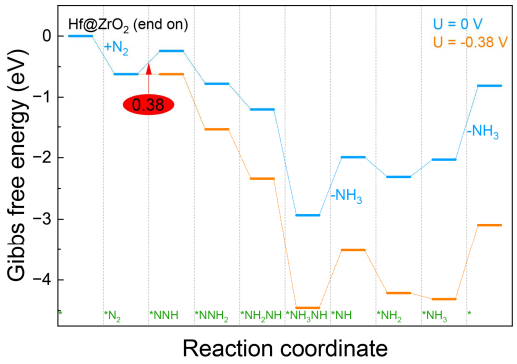

Figure S32. The free energy diagrams of Hf@ZrO_2 with end-on configuration.

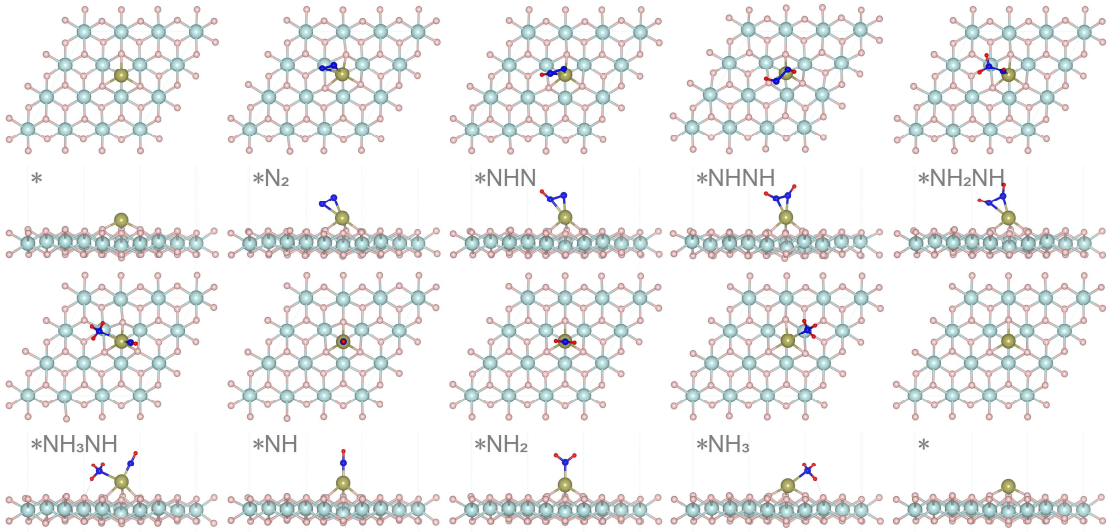

Figure S33. The NRR pathway of Hf@ZrO_2 with side-on configuration.

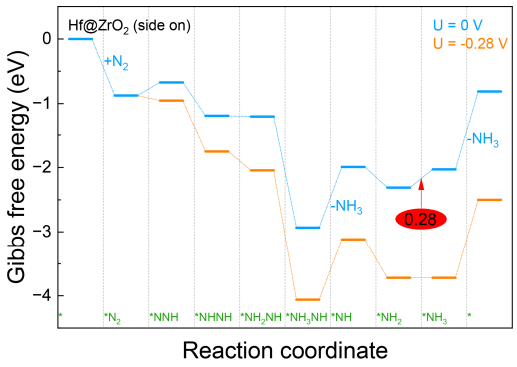

Figure S34. The free energy diagrams of Hf@ZrO_2 with side-on configuration.

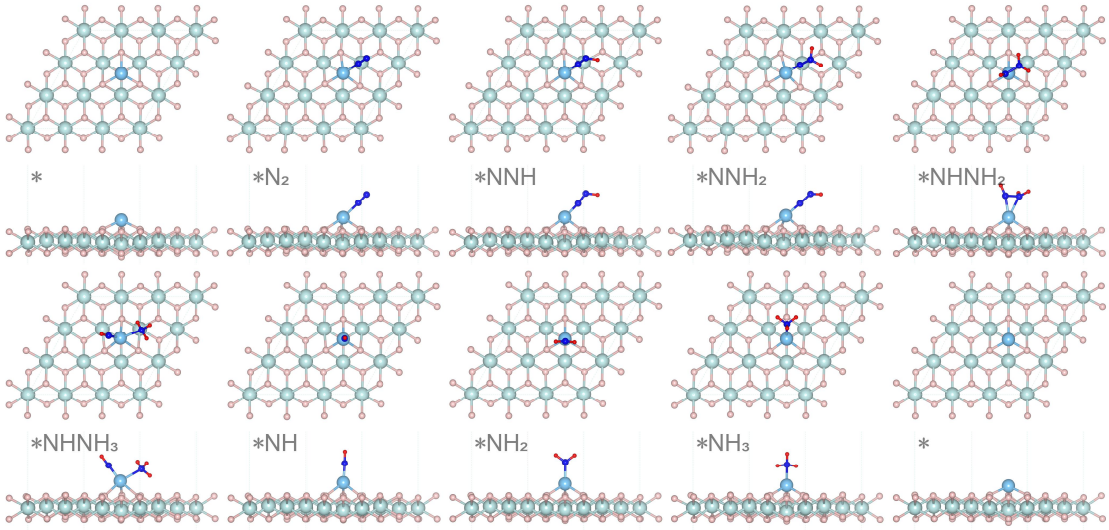

Figure S35. The NRR pathway of Ti@ZrO_2 with end-on configuration.

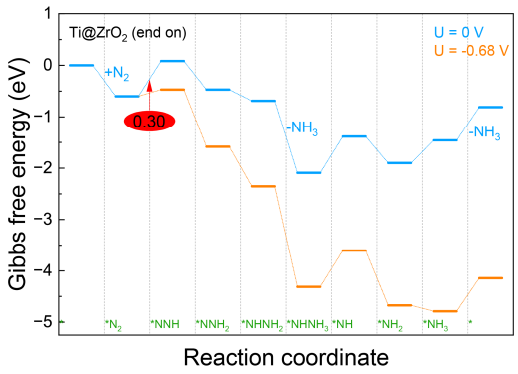

Figure S36. The free energy diagrams of Ti@ZrO_2 with end-on configuration.

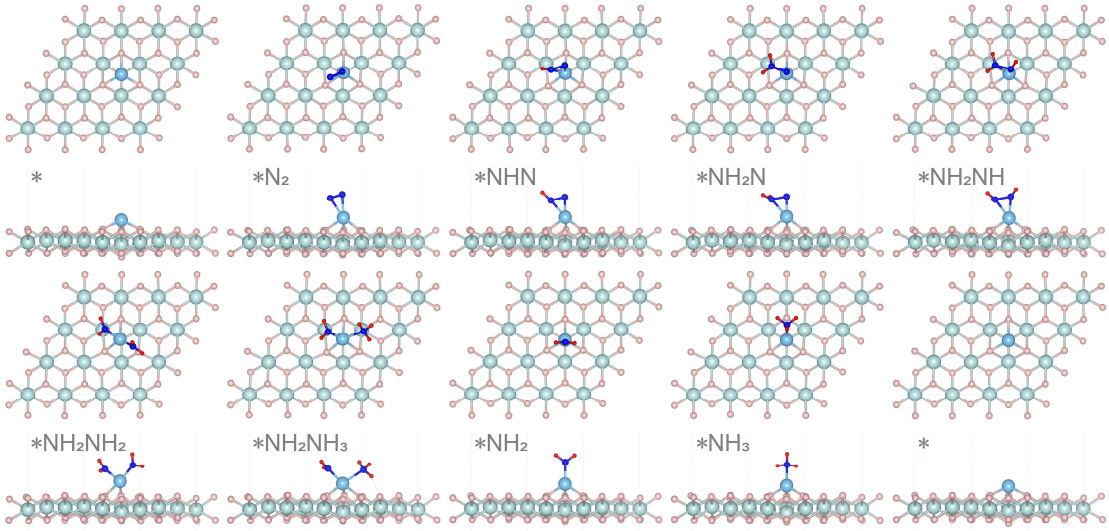

Figure S37. The NRR pathway of Ti@ZrO_2 with side-on configuration.

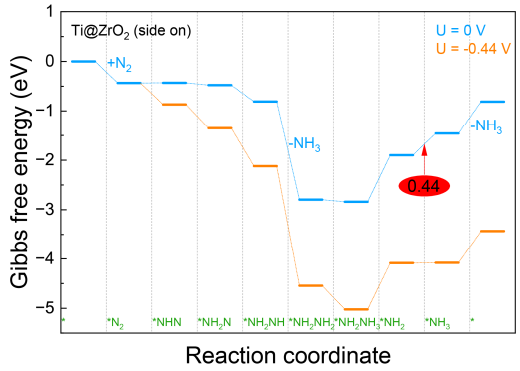

Figure S38. The free energy diagrams of Ti@ZrO_2 with side-on configuration.

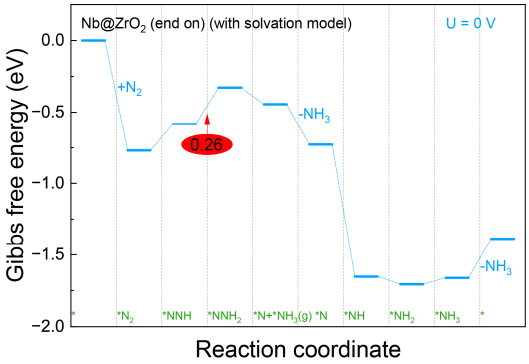

Figure S39. The free energy diagrams of Nb@ZrO_2 for end-on configuration with solvation effects.

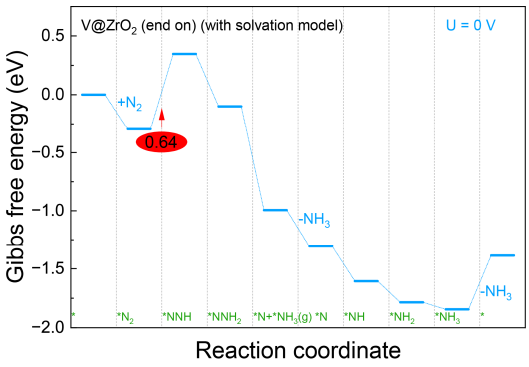

Figure S40. The free energy diagrams of V@ZrO_2 for end-on configuration with solvation effects.

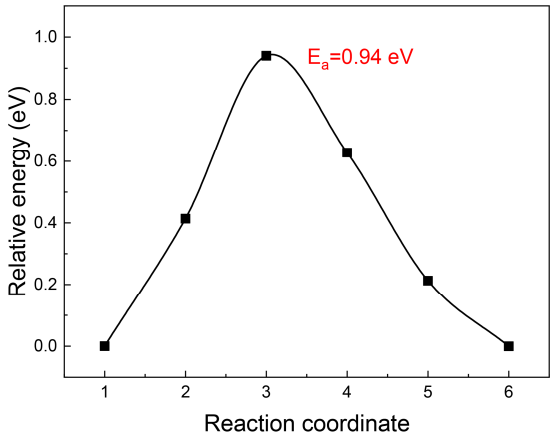

Figure S41. Migration barriers of Nb atoms on the ZrO_2 substrate.

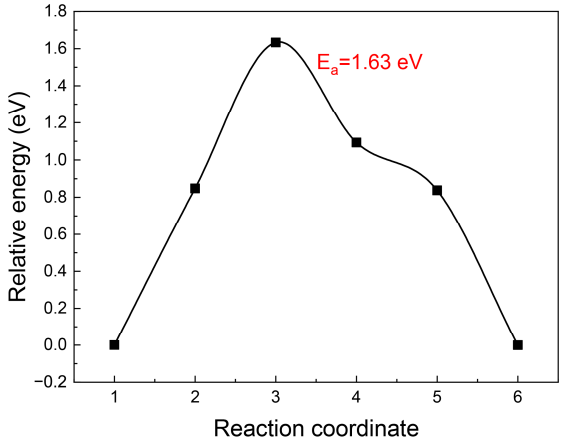

Figure S42. Migration barriers of V atoms on the ZrO_2 substrate.

Table S1. The values of feature importances, R-squared, and the predicted $-\Delta G_{max}$.

Feature importances	[0.08910426;0.11538999;0.13657659;0.42066228;0.23826688]
R-squared	0.8605754366572163
Predictions	[-0.9093431; -0.6350872; -0.5516542; -1.145729; -1.0477397; -1.4321031; -0.9211808; -0.552363; -0.4644711; -0.9414181; -1.1260527; -1.262606; -0.9755089; -1.6789716; -0.8632997; -0.4540794; -0.5874675; -0.8188272; -0.9012229; -0.9094237; -0.8704917; -1.507744]